Chiral Specificity of Doubly Resonant Sum-Frequency Generation in An Anisotropic Thin Film

ARTICLE *in* THE JOURNAL OF PHYSICAL CHEMISTRY C · JULY 2008

Impact Factor: 4.77 · DOI: 10.1021/jp7114719

2 AUTHORS:

Bertrand Busson
Université Paris-Sud 11
55 PUBLICATIONS **654** CITATIONS
SEE PROFILE

A. Tadjeddine
Université Paris-Sud 11 and CNRS
174 PUBLICATIONS **3,142** CITATIONS
SEE PROFILE

Chiral Specificity of Doubly Resonant Sum-Frequency Generation in An Anisotropic Thin Film

Bertrand Busson* and Abderrahmane Tadjeddine

Laboratoire de Chimie Physique, Université Paris-Sud 11, CNRS, Bâtiment 201 Porte 2, 91405 Orsay, France

Received: December 5, 2007; Revised Manuscript Received: March 11, 2008

The chiral specificity of infrared-visible sum-frequency generation (SFG) is investigated under doubly resonant (DR) conditions. An anisotropic thin film made of stacks of chiral supramolecular assemblies is investigated as a function of incoming and outgoing light polarizations. SFG experiments, crossed with in situ polarized absorption measurements, show that the double resonance process leads to a selection of the nonvanishing components of the chiral second-order susceptibility tensor. Specifically, it is demonstrated that a chiral component overcomes the achiral ones. This result is linked to the model for DR-SFG and to the selection rules of the vibration modes and electronic transition involved in the process.

Introduction

Chiral materials have long fascinated chemists and physicists, giving birth to a dedicated branch of science. Two enantiomers of a chiral species, mirror images of one another, have the same chemical and physical properties except when they interact with a chiral probe, such as another chiral molecule or polarized light. The specific interaction of enantiomers with light has been used as a characterization tool for many years. In linear optics, the optical activity rotates the polarization of light in an opposite direction for each enantiomer. Circular dichroism (CD) also relates to chirality. These properties arise from the fact that the chiral coefficients of the susceptibility tensor $\chi^{(1)}$ change sign with enantiomers.

Such a property can be extended to nonlinear optics.[1] Within the electric dipole approximation, second-order nonlinear processes (second harmonic generation, SHG; sum-frequency generation, SFG) require the breaking of the inversion symmetry, in other words the material must not be centrosymmetric. Chiral nonracemic samples intrinsically possess this property. This leads to effects analogous to linear optics like SHG-CD[2] and SHG-ORD but also to new effects like linear dichroism (SHG-LD[3]). SHG has long been the dedicated technique to study nonlinear optical properties of chiral samples.[4] In parallel, chiral molecular and supramolecular design aiming at the enhancement of nonlinear optical properties has grown.[5]

More recently, SFG has been used to investigate the chiral properties of chiral surfaces and bulks. When involving infrared light, SFG is able to add chemical information through the resonant excitation of molecular vibration modes. Several groups have studied the chiral specificity of SFG in liquid bulk[6–8] and debated on the origin of the signal.[9,10] Within the electric dipole approximation, rotational averaging of molecular orientations in the liquids imply that only chiral liquids may be investigated and that SHG is forbidden.[11] Furthermore, SFG intensity is weak as it requires the breaking of the adiabatic approximation. It may be enhanced when one or several beams become resonant with molecular electronic transitions.[12,13]

The situation becomes more favorable when the three-dimensional rotational averaging is broken in a thin film or a monolayer. This is the usual configuration used for most of SFG and SHG experiments. In that geometry, the chiral SFG signals have been shown to remain hard to detect, even under infrared resonant (hereafter called "singly resonant") conditions.[14] Therefore, authors take advantage of interference between chiral and achiral contributions or of doubly resonant effects[15] (defined as the double enhancement of the SFG response when both the infrared and sum-frequency wavelengths fall in the vicinity of a vibrational and an electronic transition, respectively) to access chiral components. However, $\chi^{(2)}$ in thin films with azimuthal isotropy has many vanishing components, and in such samples one loses information about the molecular in-plane response. The situation is different in oriented (i.e., anisotropic) thin films, for which the number of different coefficients increases,[16] allowing a comparison between microscopic (molecular) and macroscopic contributions.

In this article, we combine the advantages of double resonance and anisotropy in an infrared-visible SFG experiment, adding a spectroscopic dimension to previous SHG measurements on anisotropic chiral thin films (for a review, see refs 4 and 16 and references therein). The goal of this study is to distinguish between the effects of resonance, anisotropy, and chirality and to compare the values of the chiral components of the second-order nonlinear tensor $\chi^{(2)}$ to the achiral ones. We report evidence of a doubly resonant signature of chirality in an oriented thin film. The use of an anisotropic sample makes it possible to discriminate between nonlinear coefficients and show that the chiral contribution to SFG is predominant. The main coefficient is investigated as a function of the electronic and vibrational properties of the sample, and its magnitude is explained by both resonant enhancement and geometrical factors.

Experimental Section

Sample preparation has been described previously.[17] They are based on one pure enantiomer (P) of the chiral helicene bisquinone (HBQ) derivative shown in Figure 1.[18] We set the molecular axes (X^M,Y^M,Z^M) as in Figure 1. If the molecule was planar, (X^M,Z^M) would define the molecular plane. The molecule has a C_2 symmetry around the Z^M axis.

* To whom correspondence should be addressed. E-mail: Bertrand.Busson@u-psud.fr. Phone: +33 1 69 15 32 75. Fax: +33 1 69 15 33 28.

10.1021/jp7114719 CCC: $40.75
Published on Web 07/15/2008

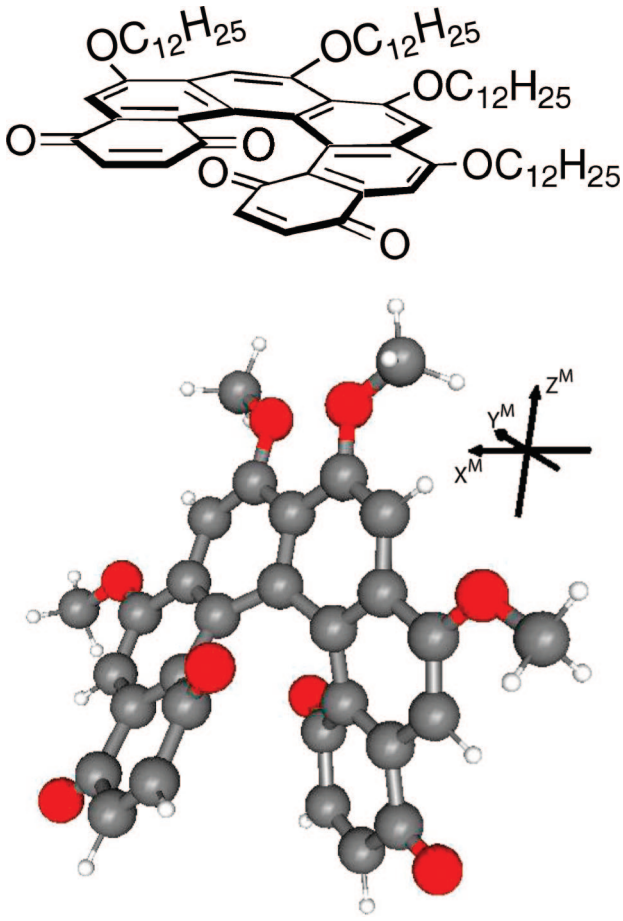

Figure 1. Top: Chemical structure of the helicene bisquinone (HBQ) molecule. Bottom: 3D structure of the simplified molecule HBQ^S.

When spread at the surface of water and compressed in a Langmuir film, these molecules form long and ordered fibers,[19–21] in which the molecular packing geometry has been debated.[22] Because of the rodlike structure of the fibers, compact Langmuir films have a C_2 symmetry with the fibers aligned parallel to the Langmuir trough's barriers. It is then possible to transfer these supramolecular structures, without disturbing the 2-fold symmetry, by a Langmuir−Blodgett vertical Y-type dipping technique onto a hydrophobic substrate (i.e., with its surface fully covered with octadecyltrichlorosilane). For this study, we have used such films made of 12 layers deposited on commercial microscope glass slides. SHG and microscopy measurements[23] show that the films are ordered and highly anisotropic. The schematic structure of the films is depicted in Figure 2. Macroscopic axes (x,y,z) are bound to the film and follow its rotation with azimuthal angle φ. The fibers are regularly aligned in an hexagonal packing, with their average orientation perpendicular to the dipping direction of the films.[20] By consideration of the probable packing of molecules inside the fibers, they stand with their edges on the outside, in other words with the Y^M axis parallel to the fiber axis. As for X^M and Z^M, the molecules are supposed to rotate regularly around Y^M along the fiber, so the distribution of molecules is isotropic as far as this rotation is concerned. In the schematic view of Figure 2, axes Y^M and y are parallel, whereas X^M and Z^M isotropically contribute to x and z. However, the fibers, although they present a net alignment parallel to the y axis on the film, show a natural angular distribution of their axes around this direction. In other words, the macroscopic average direction of the fiber axes is y, whereas individual fibers in adjacent regions (and therefore their

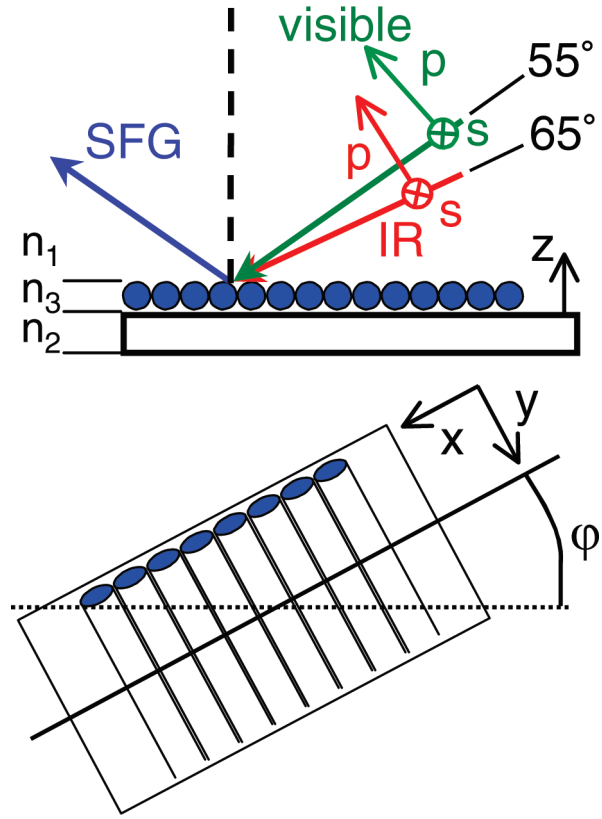

Figure 2. Schematic structure of the LB film of aggregated HBQ molecules (only one layer is drawn for clarity). Angle φ defines the azimuthal rotation ($\varphi = 0°$ for horizontal film; $\varphi = 90°$ for vertical film). Reflected and transmitted beams are not drawn for clarity.

Y^M axis) may point toward a direction in between x and y. This confers the films a 2-fold symmetry axis,[16] which we have checked on the particular case of the 12-layer film by visible reflection anisotropy spectroscopy (RAS).[24,25] The overall film symmetry is C_2 or D_2, depending whether a symmetry between two consecutive layers is induced inside the film as a consequence of the up and down Y-type deposition process. This question will be discussed below. To take the anisotropy into account, all the following spectroscopic experiments have therefore been performed on two orientations of the films, called horizontal ($\varphi = 0°$) and vertical ($\varphi = 90°$), in reference to Figure 2.

The SFG setup has been described previously,[26] with the following evolutions. The wavenumber range of the infrared optical parametric oscillator (OPO) has been extended to 1500−4000 cm^{-1}. In the probed infrared region (around 1600 cm^{-1}), the OPO bandwidth is 2 cm^{-1} with 1 μJ per pulse (∼100 μJ per train comprising around 100 pulses at 100 MHz). The infrared and visible beams, either s or p polarized, are then mixed at the probed point of the interface with angles of incidence of 65 and 55°, respectively. The SFG photons are detected in the reflection geometry by photomultipliers after polarization filtering and removal of stray light through a spectrometer. The SFG signal is normalized to the one generated by a ZnS reference crystal in order to compensate for laser fluctuations or losses during light propagation, as the 1600 cm^{-1} region is located in the middle of the strong atmospheric absorption bands due to water scissoring vibration modes.

IR absorption spectroscopy in the 400−4000 cm^{-1} range with a 4-cm^{-1} resolution was performed in a reflection geometry at 80° incidence (Nicolet Magma 560). Polarization state of light was filtered by a Specac KRS-5 polarizer. For the absorbance

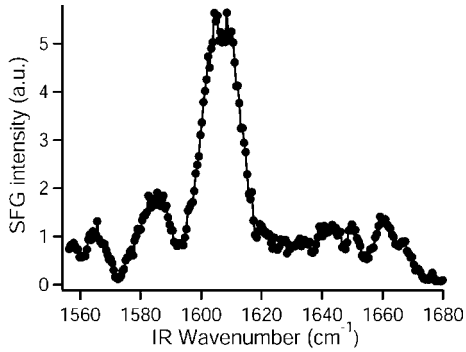

Figure 3. SFG spectrum of the horizontal 12-layer HBQ film, spp polarization combination.

determination, a bare glass slide was used as a reference. To measure small absorbance values around 1600 cm^{-1}, reference spectra of atmospheric water were recorded and subtracted from our data. To account for the marked interference feature of glass reflection due to the 1100 cm^{-1} absorption band,[27] which cannot be completely eliminated by the division process, a linear background was subtracted.

Visible absorption was performed on a laboratory Varian Cary 50 spectrometer in the 300−700 nm range in a transmission geometry (incidence on glass slide first) at 84° incidence. Input polarization state of light was filtered by a calcite Glan polarizer. A blank glass slide was used as a reference for absorbance calculations, and the absorption peak was then cleaned from both constant and long-range exponentially decreasing backgrounds. This treatment of data leaves only the resonant part of the absorption. RAS was carried out using a standard scheme[24] in the 250−800 nm range. Briefly, the light of a xenon lamp is polarized linearly before reflection on the sample surface near normal incidence. After traveling into a photoelastic modulator and an analyzer oriented at 45°, the real and imaginary parts of the anisotropic reflectivity can be recorded separately. The real part relates to anisotropic absorption. The sample was azimuthally rotated for angular analysis.

DFT calculations were carried out on a simplified model molecule (HBQ^S) where $C_{12}H_{25}$ chains are replaced with CH_3 groups (Figure 1b). We used the Gaussian package 03,[28] with B3LYP hybrid functional, 6-311++G(d,p) basis set, and a correction factor of 0.97 for calculated infrared frequencies.[29]

Results and Discussion

Figure 3 shows a typical SFG spectrum, with a spp polarization scheme for SFG-visible-IR beams, respectively. To avoid damaging the samples, the visible power was dramatically reduced to an average power between 0.5 and 1 mW (energy per pulse between 0.2 and 0.4 μJ). For the same reason, the probed point on the sample was regularly changed when successive spectra were recorded.[15] The fact that our samples absorb light in the visible and the IR during the SFG experiments (as will be detailed below) explains their fragility under the laser beam exposure. Regular check of the fact that the sample was not damaged by the laser have been made to ensure the quality of the data.

The structure is rich and complex. DFT calculations support the separation in two spectral ranges. Around 1650 cm^{-1}, molecular vibration modes mainly consist of C═O stretching of the quinone carbonyl groups. Below 1630 cm^{-1}, several C—C stretching modes of the phenyl rings create the left half of the spectrum. These findings are compatible with the literature on

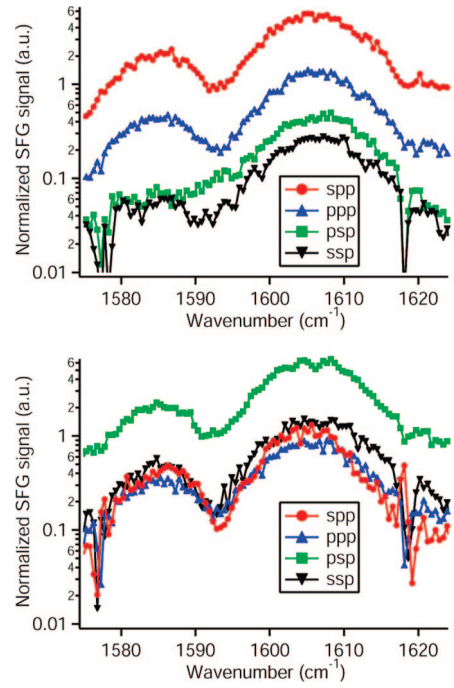

Figure 4. Comparison between SFG spectra (logarithmic scale) of the HBQ 12-layer film for the four p-polarized infrared polarization combinations. Film geometry is horizontal (top) and vertical (bottom). Spectra are not corrected from Fresnel factor effects.

fused ring quinones (see, for example, refs 30, 31, and 32 for 9,10-anthraquinone and derivatives).

Measurements were repeated with the eight polarization combinations with two orientations for the film. The first striking result is that the signals with incoming s-polarized IR are hardly measurable. More precisely, for both orientations, the signal generation in highest polarization combination involving s-polarized IR is at least 1 order of magnitude smaller than the one generated in lowest polarization scheme involving p-polarized IR. In the following, s-polarized IR combinations will be considered as approximately zero. Thus, only p-polarized IR results, focused on the highest peak, are shown in Figure 4.

The spectra show that for every sample orientation there is a major contribution overwhelming the three others, namely, spp for the horizontal film and psp for the vertical one. It is not possible to deduce all the intensity ratios between these signals, as the point on the sample had to be moved regularly in order to avoid film damaging. The homogeneity of the film surface is not good enough to ensure that the orientation distribution of the fibers is the same for every measurement, inducing a distortion of the polarization effects between the curves. Measurements have been made several times in order to have enough reproducibility on the conclusions and the major contribution has been checked carefully to avoid any artifact.

At the macroscopic level, the source of SFG is the second-order polarization, defined in the electric dipole approximation as

$$P_i^{(2)}(\omega_{SFG}) = \chi_{ijk}^{(2)} E_j^{vis}(\omega_{vis}) E_k^{IR}(\omega_{IR}) \quad (1)$$

where the $\chi^{(2)}$ tensor is the second-order susceptibility and i,j,k stand for any Cartesian coordinate x,y,z.[33] $\chi^{(2)}$ arises from a macroscopic averaging over molecular orientations of the microscopic hyperpolarizability tensor β_{IJK}, where I,J,K stand for the molecular coordinates X^M,Y^M,Z^M.[34] The hyperpolarizability is resonant with IR-active vibration modes and exhibits a Lorentzian energy profile as a function of the IR wavenum-

ber.[35] Additional factors accounting for the effective SFG activity of a mode are discussed below. Kauranen et al.[36] have shown that, in HBQ films, magnetic contributions to the second order polarization can be neglected, which justifies the electric dipole approximation in eq 1. For a film having a C_2 symmetry, there are 13 nonvanishing $\chi^{(2)}$ coefficients,[37] namely, *xxz*, *yyz*, *zzz*, *xzx*, *yzy*, *zxx*, *zyy*, *xyz*, *yxz*, *xzy*, *yzx*, *zxy*, and *zyx*. The latter six coefficients would vanish for an achiral sample and are therefore called chiral coefficients. For a film with a D_2 symmetry, only the chiral coefficients remain. It must be noted that the choice of the (*x*,*y*,*z*) axes is fixed in the case of a D_2 symmetry, as it corresponds to the three axes of symmetry of the sample. For a C_2 symmetry, however, only *z* is fixed by the symmetry; *x* and *y* are free choices. This leads some authors to consider only isotropic combinations of $\chi^{(2)}$ coefficients to account for this arbitrariness.[36] In our case, we have checked by RAS that (*x*,*y*,*z*) have been chosen along the principal axes of the film (defined by the dipping direction and the average orientation of the fibers), which makes their choice unambiguous. This also justifies the separation between chiral and achiral contributions.

For the analysis of the data of Figure 4, and to separate chirality from anisotropy effects, we follow the derivation of Maki et al.[38] for SHG and extend it to SFG. The far field SFG intensity is expressed as

$$I(\omega_{\mathrm{SFG}}) = \frac{c\,|\vec{E}(\omega_{\mathrm{SFG}})|^2}{2\pi} \tag{2}$$

In the general case, it is possible to write

$$E_{\mathrm{s/p}}(\omega_{\mathrm{SFG}}) \propto f_{\mathrm{s/p}} E_p^{\mathrm{vis}} E_p^{\mathrm{IR}} + g_{\mathrm{s/p}} E_s^{\mathrm{vis}} E_s^{\mathrm{IR}} + h_{\mathrm{s/p}} E_p^{\mathrm{vis}} E_s^{\mathrm{IR}} + m_{\mathrm{s/p}} E_s^{\mathrm{vis}} E_p^{\mathrm{IR}} \tag{3}$$

where s/p stands for the polarizations, and *f*, *g*, *h*, *m* are effective second-order susceptibilities, functions of the $\chi^{(2)}_{ijk}$ components, angles of incidence, azimuthal angle φ, and Fresnel factors.[39,40] The formalism of eq 3 makes it easy to express the SFG intensity for all the polarization schemes like, for example

$$I^{\mathrm{SFG}}_{\mathrm{psp}} \propto |m_{\mathrm{p}}|^2 \tag{4}$$

Each $\chi^{(2)}$ coefficient is weighted by optical Fresnel factors calculated in a three layer model, namely, F^{s}, $F^{\mathrm{p}_{\parallel}}$, and $F^{\mathrm{p}_{\perp}}$, where s and p refer to the beam geometry and || and ⊥ refer to the film plane. Local field corrections are neglected. We use projected Fresnel factors which include the geometrical conversion between (s,p) and (*x*,*y*,*z*) basis. This allows to work in s/p terms (which refer to the fixed incoming beams) instead of (*x*,*y*,*z*) which rotate with angle φ. As a guidance, F^{s}, $F^{\mathrm{p}_{\parallel}}$, and $F^{\mathrm{p}_{\perp}}$ relate to the usual coefficients (noted L_{xx}, L_{yy}, and L_{zz} for example in ref 41) by

$$F_i^{\mathrm{s}} = L_{yy}(\omega_i);\ F_i^{p_{\parallel}} = L_{xx}(\omega_i)\cos(\theta_i^1);\ F_i^{p_{\perp}} = L_{zz}(\omega_i)\sin(\theta_i^1) \tag{5}$$

where

$$L_{xx}(\omega_i) = \frac{2n_i^1\cos\theta_i^2}{n_i^1\cos\theta_i^2 + n_i^2\cos\theta_i^1}$$

$$L_{yy}(\omega_i) = \frac{2n_i^1\cos\theta_i^1}{n_i^1\cos\theta_i^1 + n_i^2\cos\theta_i^2}$$

$$L_{zz}(\omega_i) = \frac{2n_i^2\cos\theta_i^1}{n_i^1\cos\theta_i^2 + n_i^2\cos\theta_i^1}\left(\frac{n_i^1}{n_i^3}\right)^2 \tag{6}$$

Quantities noted n_i^j and θ_i^j mean that they are evaluated for beam *i* (frequency ω_i with $i = 1, 2, 3$, respectively, for visible, IR, and SFG) in medium $j = 1, 2, 3$, respectively, for air, glass, and HBQ film. For the calculation of the Fresnel coefficients, we use the following values for the indices of refraction: $n^1{}_i = 1$, $n^2{}_{1,3} = 1.52$ in the visible range, and $n^3{}_i = 1.57$.[17] It should be noted that the value of $n^3{}_i$ solely, but strongly, affects the *z* components of the electric fields.[41] The 1600 cm^{-1} IR wavenumber region is affected by the strong 1100 cm^{-1} absorption band of glass due to Si−O−Si stretching, which leads to a peaked dispersion curve for $n^2{}_2$ in the mid-infrared. Additionally, the refractive index strongly depends on the chemical composition and quality of the glass. We have thus chosen here the value $n^2{}_2 = 1.32$ for a standard soda-lime glass at 1600 cm^{-1}.[27]

With these notations, the coefficients of eq 1 for the horizontal sample read

$$f_p = -F_3^{\mathrm{p}_{\parallel}}F_1^{\mathrm{p}_{\parallel}}F_2^{\mathrm{p}_{\perp}}\chi^{(2)}_{xxz} - F_3^{\mathrm{p}_{\parallel}}F_1^{\mathrm{p}_{\perp}}F_2^{\mathrm{p}_{\parallel}}\chi^{(2)}_{xzx} - F_3^{\mathrm{p}_{\perp}}F_1^{\mathrm{p}_{\parallel}}F_2^{\mathrm{p}_{\parallel}}\chi^{(2)}_{zxx} - F_3^{\mathrm{p}_{\perp}}F_1^{\mathrm{p}_{\perp}}F_2^{\mathrm{p}_{\perp}}\chi^{(2)}_{zzz} \tag{7}$$

$$f_s = F_3^{\mathrm{s}}F_1^{\mathrm{p}_{\perp}}F_2^{\mathrm{p}_{\parallel}}\chi^{(2)}_{yzx} - F_3^{\mathrm{s}}F_1^{\mathrm{p}_{\parallel}}F_2^{\mathrm{p}_{\perp}}\chi^{(2)}_{yxz} \tag{8}$$

$$\mathrm{g}_p = F_3^{\mathrm{p}_{\perp}}F_1^{\mathrm{s}}F_2^{\mathrm{s}}\chi^{(2)}_{zyy};\ g_s = 0 \tag{9}$$

$$h_p = F_3^{\mathrm{p}_{\parallel}}F_1^{\mathrm{p}_{\perp}}F_2^{\mathrm{s}}\chi^{(2)}_{xzy} - F_3^{\mathrm{p}_{\perp}}F_1^{\mathrm{p}_{\parallel}}F_2^{\mathrm{s}}\chi^{(2)}_{zxy};\ h_{\mathrm{s}} = F_3^{\mathrm{s}}F_1^{\mathrm{p}_{\perp}}F_2^{\mathrm{s}}\chi^{(2)}_{yzy} \tag{10}$$

$$m_p = F_3^{\mathrm{p}_{\parallel}}F_1^{\mathrm{s}}F_2^{\mathrm{p}_{\perp}}\chi^{(2)}_{xyz} - F_3^{\mathrm{p}_{\perp}}F_1^{\mathrm{s}}F_2^{\mathrm{p}_{\parallel}}\chi^{(2)}_{zyx};\ m_{\mathrm{s}} = F_3^{\mathrm{s}}F_1^{\mathrm{s}}F_2^{\mathrm{p}_{\perp}}\chi^{(2)}_{yyz} \tag{11}$$

where

$$F_1^{\mathrm{s}} = 0.619;\ F_2^{\mathrm{s}} = 0.611;\ F_3^{\mathrm{s}} = 0.613 \tag{12}$$

$$F_1^{\mathrm{p}_{\parallel}} = 0.564;\ F_2^{\mathrm{p}_{\parallel}} = 0.478;\ F_3^{\mathrm{p}_{\parallel}} = 0.558 \tag{13}$$

$$F_1^{\mathrm{p}_{\perp}} = 0.338;\ F_2^{\mathrm{p}_{\perp}} = 0.319;\ F_3^{\mathrm{p}_{\perp}} = 0.339 \tag{14}$$

The coefficients for the vertical sample are deduced by exchanging *x* and *y* coordinates in all $\chi^{(2)}_{ijk}$ and changing the sign of the chiral components. In the following, a $\chi^{(2)}$ coefficient may be referred to as its three coordinates (e.g., *zzz* standing for $\chi^{(2)}_{zzz}$).

It is obvious from the above formulas that, in the D_2 symmetry hypothesis, the achiral polarization contributions ppp and ssp should vanish, which is not the case. Therefore, the film symmetry does not seem to be D_2. In the case of an anisotropic chiral sample, bulk SFG is symmetry-allowed, and the response therefore comprises surface and bulk contributions. The condition for the effective generation of bulk signal is that the thickness of the film is lower than the coherence length, defined as $\pi/\Delta k$, where Δk is the wave vector mismatch. For HBQ films, the thickness has been evaluated to 1.95 nm per molecular layer by SHG.[17] An estimate of the coherence length with a refractive index of 1.57 and the experimental geometry described above gives $L_c \approx 92$ nm, almost four times the thickness of the film (23.4 nm). It could be imagined that the bulk has a D_2 symmetry, whereas the surface is only C_2. However, for the case of a 12-layer film, the SFG intensity being

proportional to the squared density of molecules,[41] it is reasonable to consider that the surface signal is overwhelmed by the bulk one, which makes the hypothesis of different symmetries incompatible with the experimental data. Thus the data analysis will be carried out according to a C_2 symmetry and a bulk origin for the sum frequency signal.

At this stage, the tensor decomposition already shows that the two main contributions to Figure 3 are only related to chirality and would vanish if the sample was achiral. A more accurate analysis of the major $\chi^{(2)}$ coefficients is detailed in the following. However, the tensor decomposition together with the values of the Fresnel factors do not by themselves account for the vanishing combinations involving s-polarized IR, in particular g_p and h_s. As a consequence, we deduce from eqs 9 and 10 that *zxx*, *xzx*, *zyy*, and *yzy* (respectively, pss and sps polarization schemes in the horizontal and vertical configurations) vanish. The vanishing of h_p may arise from the vanishing of *xzy*, *zxy*, *yzx*, and *zyx* coefficients, but by consideration that they have close values of their Fresnel factors, only the equalities $xzy = zxy$ and of $yzx = zyx$ are necessary to eliminate the pps combination. It is not possible at this stage to discriminate between these two possibilities.

To go further into the interpretation of the data, we need additional experimental information on the dispersion and geometry of the nonlinear optical coefficients. By consideration that the properties of HBQ in LB films are not comparable to those of molecules in solution, all the complementary experiments have to be performed on the same 12-layer film as has been used for SFG.

At the molecular level, the IR-resonant SFG hyperpolarizability is proportional to the IR transition moment of a given vibration mode, more precisely

$$\beta_{ijk} \propto \left(\frac{\partial \mu_k}{\partial Q_l}\right)_{Q_l=0} \tag{15}$$

where μ is the dipole moment, l numbers the IR mode, and Q stands for the vibration coordinate.[35] It is therefore crucial to know the dependence of the IR activity of the vibration modes on the Cartesian coordinates in the investigated energy range. To have access to this information, we performed IR absorption experiments at grazing incidence, which allows to probe both the in-plane and z components of the absorption. Furthermore, we used polarized input beams and tested both horizontal and vertical geometries. In such a configuration, the input beams with p polarization outside the sample are polarized quasiperpendicularly to the surface.

The data are shown in Figure 5. The spectra illustrate the fact that linear optical methods, contrary to SFG, are not able to measure a clear difference between horizontal and vertical film. This is due to the fact that, for a disordered sample, linear spectroscopies sum up the contributions of absorbers. If the disorder is rather large, the difference between an isotropic and a disordered sample is small. On the contrary, SFG is very sensitive to the local organization and to the net orientation of the fibers. In addition, linear methods use wide light beams which average the response over large areas and do not correctly account for the local order.

The shape of the top graph in Figure 5 ("negative absorbance") is explained by optical effects related to Fresnel contributions and the propagation of the electromagnetic field inside the sample. A detailed analysis of such reflectivity measurements on a three-layer model can be found in ref 42.[42] It shows that, for external incidence, the s polarization leads to a negative absorbance. The p polarization spectrum is the sum

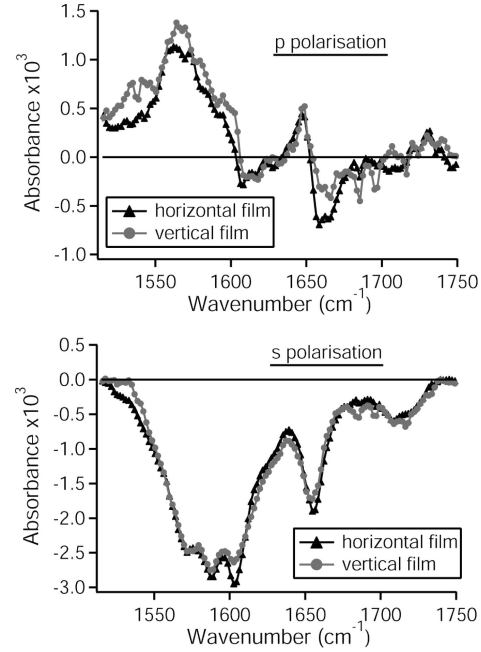

Figure 5. Background-corrected infrared absorption spectrum of the HBQ 12-layer film in the horizontal and vertical geometries. Top: beam is p polarized. Bottom: beam is s polarized.

of the $p_{\parallel}$ and $p_{\perp}$ contributions. These contributions behave in a more complex way than is explained in ref 42, as they change sign when the angle of incidence crosses the Brewster angle of the substrate. For grazing incidence, the $p_{\parallel}$ contribution is thus positive, whereas the $p_{\perp}$ is negative, and their sum is responsible for the positive-negative interference shape. The negative parts of the spectra are thus a direct evidence of the activity of the vibration modes along the z direction. The four modes seen in SFG are present in Figure 5 (bottom). The resolution and signal-to-noise ratio do not allow to evidence them in the top part of Figure 5, although the C═O stretching mode and at least one phenyl C—C stretching mode are clearly seen. The other C—C stretching modes compose the broad peak between 1550 and 1600 cm^{-1}, although the interference between these nearby modes does not allow to separate their respective positive and negative parts. However, it is clear that the modes involved in the SFG process are active both in and out of the plane of the film, and that no obvious in-plane anisotropy is measurable.

As a consequence, the infrared part of the $\chi^{(2)}_{ijk}$, indexed by k, should not vanish for any value of k. In other words, the transition moment has a nonzero value for $k = x$, y, and z. This shows that the IR resonance is not responsible for the vanishing of s-polarized contributions to SFG. The consequence is straightforward: the vanishing of *zxx*, *xzx*, *zyy*, and *yzy* is due to the visible range behavior (i.e., the first two indices). This in turn implies that coefficients *zxy*, *xzy*, *zyx*, and *yzx* also vanish for the same reason. The essential consequence of these simplifications is that the number of non vanishing coefficients has considerably lowered, as only *xxz*, *xyz*, *yxz*, *yyz*, and *zzz* remain. Considering that the *zzz* contribution is heavily lowered by Fresnel coefficients effects and may therefore be neglected in ppp generation, it appears that every measured SFG polarization combination is by far related to a single major $\chi^{(2)}$ coefficient (Table 1).

As mentioned before, the inhomogeneity of the sample does not allow a direct measurement of the absolute value of these coefficients. However, from the comparison of several sets of data, we may draw the following conclusions:

TABLE 1: Equivalence between Nonvanishing Polarization Combinations for SFG Spectra, Effective Second-Order Susceptibility Coefficient, and Main Second-Order Susceptibility Contribution

polarization combination	coefficient	horizontal film	vertical film
ppp	f_p	*xxz*	*yyz*
spp	f_s	*yxz*	*xyz*
psp	m_p	*xyz*	*yxz*
ssp	m_s	*yyz*	*xxz*

First, the main contribution to SFG is the *yxz* coefficient, and it is a signature of chirality. The fact that the main coefficient is chiral is to be related to the same conclusion drawn by SHG on a similar sample.[36] It must be noted that, on that experiment, the SHG was resonant but not the fundamental, as will be shown below from the analysis of the optical response of the film in visible range;

Second, all remaining coefficients share a *z* component for the IR beam. That shows that the whole set of SFG data is scaled by the common $F_2^{p\perp}$ Fresnel factor, which consequently implies that the exact value of the refractive index n_3 for the HBQ film has no consequence on the ratios between the various polarization combinations.

The vanishing of 8 of the 13 $\chi^{(2)}$ components is still to be explained. An infrared-resonant cause being ruled out, we turn to the study of the properties of the films in the visible range. As for the visible part of $\chi^{(2)}$, we have to consider two cases, namely, singly and doubly resonant processes. In the singly resonant case, the molecular hyperpolarizability related to a given IR-active mode is proportional to the Raman transition moment of that mode

$$\beta_{ijk} \propto \sum_{l}^{\text{IR active modes}} \frac{\left(\frac{\partial \mu_k^{IR}}{\partial Q_l}\right)_{Q_l=0}\left(\frac{\partial \alpha_{ij}}{\partial Q_l}\right)_{Q_l=0}}{\omega_{IR} - \omega_l + i\Gamma_l} \qquad (16)$$

where α stands for the molecular polarizability.[35]

No Raman signal could be measured on the HBQ film with three excitation wavelengths of 514.4, 785, and 1064 nm, mainly because the weak Raman intensity from the molecules is overwhelmed by a huge background from the glass. This means that the singly resonant hypothesis cannot be directly tested experimentally. However, we can get some indirect information from the previous IR absorption data.

For a C_2 symmetry molecule, only two types of vibrations exist (A and B), for which the selection rules are the following.[43] A modes are totally symmetric; they can only be excited by infrared light parallel to the C_2 axis (Z^M, see Figure 1). In that case, the Raman activity is related to (omitting superscripts M for clarity) α_{XX}, α_{XY}, α_{YX}, α_{YY}, and α_{ZZ} components of the polarizability. B modes on the contrary are antisymmetric, which implies that their IR activity relates to light polarized in the (X^M,Y^M) plane, whereas allowed Raman transitions concern the four components of the polarizability which involve a Z^M coordinate (X^MZ^M, Y^MZ^M, Z^MX^M, and Z^MY^M). The molecular response is then averaged over orientational distribution to create the macroscopic response of the sample. As a result of the structure of the films and the rotational averaging detailed above, the A modes have a nonvanishing vibrational component along *x*, *y*, and *z*, as do B modes vibrating along X^M. On the contrary, B modes vibrating along Y^M have a component only along *x* and *y*, which contradicts experimental evidence. As for the polarizability, the same reasoning shows that for A modes, a nonvanishing molecular α_{XX} term for example is sufficient to lead to nonvanishing contributions for all the eight terms of the macroscopic polarizability. The conclusion is similar for B modes when considering α_{XZ} or α_{ZX} terms. In other words, either A or B IR-active modes should lead to resonant contributions to $\chi^{(2)}$, which are not experimentally measured. In addition, it is likely that the molecular symmetry fades due to the supramolecular arrangement, and thus the infrared (and Raman) selection rules soften. This reinforces the previous conclusion and therefore the singly resonant model seems unable to account for the SFG experimental data.

We thus have to turn to the hypothesis of a doubly resonant SFG process, for which the photons in the visible range excite an electronic transition of the sample. HBQ molecules have been shown to exhibit a clear resonance in their absorption spectrum between 400 and 600 nm when deposited on LB films.[21] This energy range contains the visible and SFG (around 489 nm) wavelengths involved in the present experiments. This resonance increases when the HBQ molecules aggregate inside the fibers.[18] It directly relates to the molecular dimerization, or even multimerization, process, which favors the hypothesis of an excitonic coupling origin.

For doubly resonant SFG, the Raman polarizability becomes resonant. Under proper approximations (Born−Oppenheimer, Franck−Condon, harmonic vibrations, undistorted vibrational levels), the SFG hyperpolarizability can be written as[44]

$$\beta_{ijk} \propto \mu_i^{elec}\mu_j^{elec} \sum_{l}^{\text{IR active modes}} \frac{D_l}{\omega_{IR} - \omega_l + i\Gamma_l}\left(\frac{\partial \mu_k^{IR}}{\partial Q_l}\right)_{Q_l=0} \qquad (17)$$

where D_l stands for the energy-dependent resonant factors, which sum up all the contributions of the vibrational levels of the electronic excited state, and is proportional to the electron vibration coupling constant of mode l. Also to be noted that, in the Born−Oppenheimer approximation, only totally symmetric vibration modes may be efficiently excited in a DR-SFG process.[45] The enhancement factors due to resonances do not depend on the polarizations of the beams, only on the energies involved.

The above-mentioned DFT calculations show that it is possible to locate at least four totally symmetric modes in the 1550−1665 cm^{-1} range with significant IR activity. As explained above, such vibration modes will, after averaging over the molecular orientations, give rise to infrared activity along *x*, *y*, and *z*. Compared to the singly resonant case, the difference in selection rules lies in the μ_{ij} factors. As for vibration modes, electronic transitions have either A or B character, with the same geometrical implications on their transition moments (i.e., along Z^M and in the (X^M,Y^M) plane respectively). After orientation averaging, a transition along X^M or Z^M may occur by interaction with light polarized along *x*, *y*, or *z*. A transition oriented along Y^M may only be excited by light polarized in the (*x*,*y*) plane. We performed polarized visible absorption measurements on the HBQ film to study the orientation of the electronic transition and therefore test the doubly resonant hypothesis. The data are shown in Figure 6.

The absorption peak arises from the excitation of the previously mentioned electronic level. Its width accounts for the large inhomogeneous broadening of this transition, to be related to the inhomogeneity of the samples. The long high-energy tail, responsible for the asymmetry of the peak, is due to the vibronic structure, unresolved for the same reason. Together with the peak width, this asymmetric tail makes it difficult to precisely locate the peak maximum and thus the energy of the transition. However, this vibronic tail supports the hypothesis of a strong electron-vibration coupling, which

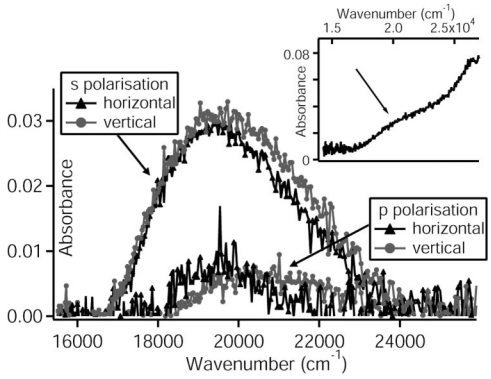

Figure 6. Background-corrected visible absorption spectrum of the HBQ 12-layer film in the horizontal and vertical geometries. Beam is p polarized (lower curves) or s polarized (upper curves). Insert shows a noncorrected spectrum (p polarized, vertical film); absorption peak is indicated by an arrow.

in turns implies that the double resonance is possible in this system for many IR modes. The information on whether the four modes under the present study exhibit double resonance phenomena cannot be extracted from the data due to the lack of resolution of the electronic structure.

The p-polarized low absorption shows that the electronic transition lies in the film plane as it is almost not excited by light polarized along the film normal. In fact, its very low height makes it even difficult to correctly remove the exponential background (example of a noncorrected spectrum is illustrated in the insert of Figure 6). Compared to the s-polarized curves, the levels of p-polarized curves may appear surprisingly low, as they encompass a common in-plane contribution, with an angle of incidence $\theta^3 = 39.3°$ inside the film. Even without undertaking a complete calculation of the four-layer system (air−glass−film−air), one should keep in mind that multiple reflections at the HBQ−air boundary (taking into account that the reflection coefficient for p polarization reaches 0.65 for a plane and nondiffusive interface) induce a reduction of the parallel component of the electric field for p-polarized light traveling inside the HBQ layer. Specifically, by consideration of the three-layer system glass−film−air, the ratio between parallel and perpendicular components in p polarization inside the film can be approximated by[38]

$$R_p = \frac{E_{p_\perp}}{E_{p_\parallel}} \approx \frac{1 + r_p^{31}}{1 - r_p^{31}} \frac{\sin(\theta^3)}{\cos(\theta^3)} = 4.71 \frac{\sin(\theta^3)}{\cos(\theta^3)} = 3.86 \quad (18)$$

where r_p^{31} is the ratio of the reflected amplitudes between media 3 and 1 for p polarization. The p-polarized light probes almost four times more perpendicular than in-plane absorption. And still the peak is much lower than for pure in-plane s polarization. The in-plane orientation of the transition moment of the electronic transition is therefore demonstrated.

The consequences of this experimental evidence are 2-fold. First, it validates the doubly resonant hypothesis and explains the vanishing of the IR s-polarized SFG signals. According to eq 17 and after averaging over molecular orientations, the in-plane selection rule for μ^{elec} restricts the doubly resonant $\chi^{(2)}_{ijk}$ to *xxk*, *xyk*, *yxk*, and *yyk*. Seen the list of nonvanishing coefficients in the C_2 symmetry, this implies that $k = z$, and consequently only p-polarized infrared light may give birth to such a doubly resonant SFG process. It also validates the hypothesis to neglect the *zzz* coefficient in the ppp polarization scheme. This scenario matches the SFG, IR absorption, and visible absorption data of Figures 4, 5, and 6. As the singly resonant model was not able to account for these experimental features, this analysis proves the double resonance. It also proves that the selection rules for nonvanishing SFG contributions in this study are a direct consequence of the double resonance, together with the properties of the vibrational and electronic transitions involved. The model of eq 17 does not explicitly take into account chiral effects, which raises questions about its relevance to describe the present data, as discussed below. However, should another description of the doubly resonant chiral effect be used, it would still include a dependence on the electronic transitions moments μ^{elec} and accordingly on their in-plane selection rule. As a consequence, the above conclusions would be the same. In the analysis of the SFG data, we have not taken into account the effects of absorption of the visible beam and reabsorption of the SF generated light inside the film. It has been shown in an SHG experiment[17] that absorption must be explicitly introduced to quantitatively fit the experimental data. In particular, the anisotropy of SF light reabsorption must affect the measured ratios between polarization combinations of Figure 4. However, it seems unlikely that this phenomenon accounts by itself for the domination of *yxz* coefficient.

Second, at the molecular level, the electronic transition must be mainly oriented along Y^M (and therefore of antisymmetric B-type) to create an in-plane macroscopic transition after orientational averaging. More accurately, a microscopic electronic transition along Y^M will lead to absorption along y only in the limit case of perfectly aligned fibers. For the structure involving disorder in the (*x*,*y*) plane with a net y alignment, the absorption must still show an anisotropy favoring absorption along *y*. In Figure 6, the absorption anisotropy in the film plane seems low, for the same reasons as those explained above for the IR experiments. To get a more accurate view on that issue, we performed RAS measurements, which have the advantage to directly measure the anisotropy without calculating the difference between two spectra. They show a slight anisotropy in the 500-nm region indeed. More precisely, the maxima and minima of anisotropic absorption measured as a function of azimuthal angle match the *x* and *y* axes of the film with an accuracy of a few degrees, confirming the definition of the principal axes, with a preferred absorption along the *y* axis of the film, which correctly matches the above scenario. It is interesting to relate this to the fact that the enhancement of the electronic transition by excitonic coupling is a direct consequence of the interaction between HBQ monomers inside the fibers, the direction of the coupling being parallel to the orientation of the transition. It shows that the deformation of the electron cloud due to the coupling between molecules mainly relates to the line linking them.

Following the model of eq 17, there should be no difference between $\chi^{(2)}_{xyz}$ and $\chi^{(2)}_{yxz}$ in the doubly resonant case, even after orientational averaging. The present experiments show that it is far from being the case. This may be due to the fact that the model fails to take properly into account the purely chiral effects. One way to improve the model, and account for a nonvanishing antisymmetric part of the electronic response, is to include non adiabatic corrections (i.e., beyond the Born−Oppenheimer approximation) as in ref 13. However, such higher order corrections are expected to remain weak, even when they resonate with electronic transitions. Furthermore, they introduce a new set of unknown coupling constants due to vibronic interaction between electronic states, which makes the conclusions of the model difficult to quantify.

The origin of chirality and the different families into which the chiral species may be classified, in relation to their nonlinear

optical properties, has been the subject of several literature pieces.[5,46–48] The origin of the chirality of HBQ molecules and films and the link to their nonlinear optical properties have been debated in this frame.[47] In that particular case, the question of a different origin for the chirality of individual molecules and supramolecular aggregates is still open. The nature of the vanishing and nonvanishing components of the $\chi^{(2)}$ tensors, including the ones involving magnetic contributions, plays a key role in this analysis. To the best of our knowledge, all the SHG and SFG experiments performed on HBQ films (including derivatives with analogous properties[49]) generated a radiation at an energy corresponding to that of the transition appearing in Figure 6 and were therefore potentially resonant with it. The results of the present study emphasize the importance of this resonance in the amplitude of the tensor components. It appears that the model for the chirality of HBQ films must take this electronic resonance into account, as it plays an essential role in the second harmonic and sum frequency generations, and partly conditions the relative values of $\chi^{(2)}$ coefficients. More dedicated studies may help improving the knowledge on that subject: first on nonaggregated molecules, for example by hyper-Rayleigh scattering in solution, in order to access the hyperpolarisabilities of single molecules; second, on aggregated samples (anisotropic Langmuir or Langmuir−Blodgett films) but out of the resonant range (for example for SHG or SFG radiation below 17000 cm^{-1}). This should lead to a better discrimination between the models for the origin of chirality of the single and aggregated HBQ species.

Conclusion

We have shown that highly anisotropic chiral thin films give rise to strong IR-resonant SFG spectra. The polarization analysis of SFG data, coupled to polarized linear optical spectroscopic techniques and modeling of the chemical structure inside the films, shows that the SFG process is doubly resonant with IR-active totally symmetric vibration modes and an electronic transition related to the molecular coupling. The doubly resonant effect strongly conditions the selection rules for the SFG experiments, leading in particular to negligible IR s-polarized spectra. This study is a step toward a complete quantification of the relative values of the $\chi^{(2)}$ chiral and achiral components, and their dispersions in the probed spectral ranges, which will allow a deeper insight into the origin of chirality of such systems; an improvement of the experimental procedure for that purpose is under study. After averaging over molecular orientations, accounting for both the structure of the fibers and their disorder inside the films, the coupled spectroscopies show that the vibration modes involved have their transition moments directed along the C_2 symmetry axis of the molecule, whereas the electronic transition is aligned along the axis linking the molecules. Additionally, it has been shown that the main source of SFG signal is related to chirality and that the model of ref 44 used to described doubly resonant SFG is probably not specific enough to account for chiral samples. Finally, these experiments suggest that the model describing the chirality of helicene bisquinone fibers may be rather complex, as a consequence of electronic resonance effects.

Acknowledgment. We acknowledge the contribution of T. Katz and C. Nuckolls for synthesizing the HBQ molecules. IR absorption measurements were performed thanks to P. Dumas, Raman measurements thanks to F. Villain and C. Roselli, and RAS measurements thanks to N. Witkowski and G. Bussetti. We acknowledge the help of P. Archirel and P. Maître for DFT calculations. We also warmly thank M. Kauranen for introducing the authors to this research field, F. Vidal and F. Hache for fruitful discussions.

References and Notes

(1) Byers, J. D.; Yee, H. I.; Petralli-Mallow, T.; Hicks, J. M. *Phys. Rev. B* **1994**, *49*, 14643–14647.
(2) Petralli-Mallow, T.; Wong, T. M.; Byers, J. D.; Yee, H. I.; Hicks, J. M. *J. Phys. Chem.* **1993**, *97*, 1383–1388.
(3) Verbiest, T.; Kauranen, M.; Maki, J. J.; Teerenstra, M. N.; Schouten, A. J.; Nolte, R. J. M.; Persoons, A. *J. Chem. Phys.* **1995**, *103*, 8296–8298.
(4) Sioncke, S.; Verbiest, T.; Persoons, A. *Mater. Sci. Eng., R* **2003**, *42*, 115–155.
(5) Simpson, G. J. *Chem. Phys. Chem.* **2004**, *5*, 1301–1310.
(6) Rentzepis, P. M.; Giordmaine, J. A.; Wecht, K. W. *Phys. Rev. Lett.* **1966**, *16*, 792–794.
(7) Shkurinov, A. P.; Dubrovskii, A. V.; Koroteev, N. I. *Phys. Rev. Lett.* **1993**, *70*, 1085–1088.
(8) Belkin, M. A.; Kulakov, T. A.; Ernst, K. H.; Yan, L.; Shen, Y. R. *Phys. Rev. Lett.* **2000**, *85*, 4474–4477.
(9) Fischer, P.; Wiersma, D. S.; Righini, R.; Champagne, B.; Buckhingham, A. D. *Phys. Rev. Lett.* **2000**, *85*, 4253–4256.
(10) Fischer, P.; Beckwitt, K.; Wise, F. W.; Albrecht, A. C. *Chem. Phys. Lett.* **2002**, *352*, 463–468.
(11) Fischer, P.; Hache, F. *Chirality* **2005**, *17*, 421–437.
(12) Fischer, P.; Wise, F. W.; Albrecht, A. C. *J. Phys. Chem. A* **2003**, *107*, 8232–8238.
(13) Belkin, M. A.; Shen, Y. R. *Phys. Rev. Lett.* **2003**, *91*, 213907.
(14) Wang, J.; Chen, X.; Clarke, M. L.; Chen, Z. *Proc. Natl. Acad. Sci. USA* **2005**, *102*, 4978–4983.
(15) Oh-e, M.; Yokoyama, H.; Yorozuva, S.; Akagi, K.; Belkin, M. A.; Shen, Y. R. *Phys. Rev. Lett.* **2004**, *93*, 267402.
(16) Verbiest, T.; Van Elshocht, S.; Kauranen, M.; Hellemans, L.; Snauwaert, J.; Nuckolls, C.; Katz, T. J.; Persoons, A. *Science* **1998**, *282*, 913–915.
(17) Busson, B.; Kauranen, M.; Nuckolls, C.; Katz, T. J.; Persoons, A. *Phys. Rev. Lett.* **2000**, *84*, 79–82.
(18) Nuckolls, C.; Katz, T. J.; Katz, G.; Collings, P. J.; Castellanos, L. *J. Am. Chem. Soc.* **1999**, *121*, 79–88.
(19) Nuckolls, C.; Katz, T. J.; Castellanos, L. *J. Am. Chem. Soc.* **1996**, *118*, 3767–3768.
(20) Lovinger, A. J.; Nuckolls, C.; Katz, T. J. *J. Am. Chem. Soc.* **1998**, *120*, 264–268.
(21) Nuckolls, C.; Katz, T. J.; Verbiest, T.; Van Elshocht, S.; Kuball, H. G.; Kiesewalter, S.; Lovinger, A. J.; Persoons, A. *J. Am. Chem. Soc.* **1998**, *120*, 8656–8660.
(22) Choi, H. S.; Kim, K. S. *J. Phys. Chem. B* **2000**, *104*, 11006–11009.
(23) Van Elshocht, S.; Verbiest, T.; de Schaetzen, G.; Hellemans, L.; Phillips, K. E. S.; Nuckolls, C.; Katz, T. J.; Persoons, A. *Chem. Phys. Lett.* **2000**, *323*, 340–344.
(24) Aspnes, D. E.; Harbison, J. P.; Studna, A. A.; Florez, L. T. *Appl. Phys. Lett.* **1988**, *52*, 957–959.
(25) Weightman, P.; Martin, D. S.; Cole, R. J.; Farrell, T. *Rep. Prog. Phys.* **2005**, *68*, 1251–1341.
(26) Humbert, C.; Busson, B.; Abid, J. P.; Six, C.; Girault, H. H.; Tadjeddine, A. *Electrochim. Acta* **2005**, *50*, 3101–3110.
(27) Worrell, C. A. *J. Mater. Sci.* **1986**, *21*, 781–787.
(28) Frisch, M. J.; Trucks, G. W.; Schlegel, H. B.; Scuseria, G. E.; Robb, M. A.; Cheeseman, J. R.; Montgomery, J. A., Jr.; Vreven, T.; Kudin, K. N.; Burant, J. C.; Millam, J. M.; Iyengar, S. S.; Tomasi, J.; Barone, V.; Mennucci, B.; Cossi, M.; Scalmani, G.; Rega, N.; Petersson, G. A.; Nakatsuji, H.; Hada, M.; Ehara, M.; Toyota, K.; Fukuda, R.; Hasegawa, J.; Ishida, M.; Nakajima, T.; Honda, Y.; Kitao, O.; Nakai, H.; Klene, M.; Li, X.; Knox, J. E.; Hratchian, H. P.; Cross, J. B.; Bakken, V.; Adamo, C.; Jaramillo, J.; Gomperts, R.; Stratmann, R. E.; Yazyev, O.; Austin, A. J.; Cammi, R.; Pomelli, C.; Ochterski, J. W.; Ayala, P. Y.; Morokuma, K.; Voth, G. A.; Salvador, P.; Dannenberg, J. J.; Zakrzewski, V. G.; Dapprich, S.; Daniels, A. D.; Strain, M. C.; Farkas, O.; Malick, D. K.; Rabuck, A. D.; Raghavachari, K.; Foresman, J. B.; Ortiz, J. V.; Cui, Q.; Baboul, A. G.; Clifford, S.; Cioslowski, J.; Stefanov, B. B.; Liu, G.; Liashenko, A.; Piskorz, P.; Komaromi, I.; Martin, R. L.; Fox, D. J.; Keith, T.; Al-Laham, M. A.; Peng, C. Y.; Nanayakkara, A.; Challacombe, M.; Gill, P. M. W.; Johnson, B.; Chen, W.; Wong, M. W.; Gonzalez, C.; Pople, J. A. *Gaussian 03,* revision C.02; Gaussian, Inc.: Wallingford, CT, 2004.
(29) Halls, M. D.; Velkovski, J.; Schlegel, H. B. *Theor. Chem. Acc.* **2001**, *105*, 413–421.
(30) Pecile, C.; Lunelli, B. *J. Chem. Phys.* **1967**, *46*, 2109–2118.
(31) Lehmann, K. K.; Smolarek, J.; Khalil, O. S.; Goodman, L. *J. Phys. Chem.* **1979**, *83*, 1200–1205.
(32) Han, S. W.; Ha, T. H.; Kim, C. H.; Kim, K. *Langmuir* **1998**, *14*, 6113–6120.

(33) Boyd, R. W. *Nonlinear optics*; Academic Press: San Diego, CA, 2003.
(34) Shen, Y. R. *The principles of nonlinear optics*; Wiley & Sons: New York, NY, 1984.
(35) Lin, S. H.; Villaeys, A. A. *Phys. Rev. A* **1994**, *50*, 5134–5144.
(36) Kauranen, M.; Van Elshocht, S.; Verbiest, T.; Persoons, A. *J. Chem. Phys.* **2000**, *112*, 1497–1502.
(37) Giordmaine, J. A. *Phys. Rev.* **1965**, *138*, 1599–1606.
(38) Maki, J. J.; Kauranen, M.; Persoons, A. *Phys. Rev. B* **1995**, *51*, 1425–1434.
(39) Born, M.; Wolf, E. *Principles of optics*; Cambridge University Press: Cambridge, UK, 1999.
(40) Heinz, T. F. In *Nonlinear Surface Electromagnetic Phenomena*; Ponath, H.-E.; Stegeman, G. I. Ed.; Elsevier Science Publishers: Amsterdam, NL, 1991; pp 353−416.
(41) Zhuang, X.; Miranda, P. B.; Kim, D.; Shen, Y. R. *Phys. Rev. B* **1999**, *59*, 12632–12640.
(42) Chabal, Y. *Surf. Sci. Rep.* **1988**, *8*, 211–357.
(43) Moad, A. J.; Simpson, G. J. *J. Phys. Chem. B* **2004**, *108*, 3548–3562.
(44) Hayashi, M.; Lin, S. H.; Raschke, M. B.; Shen, Y. R. *J. Phys. Chem. A* **2002**, *106*, 2271–2282.
(45) Herzberg, G. *Molecular spectra and molecular structure, volume III*; Krieger Publishing Company: Malabar, FL, 1991.
(46) Schanne-Klein, M. C.; Mesnil, H.; Boulesteix, T.; Hache, F. *Rec. Res. Devel. Chem. Phys.* **2003**, *4*, 487–517.
(47) Hache, F.; Mesnil, H.; Schanne-Klein, M. C. *J. Chem. Phys.* **2001**, *115*, 6707–6715.
(48) Maki, J. J.; Persoons, A. *J. Chem. Phys.* **1996**, *104*, 9340–9348.
(49) Sioncke, S.; Van Elshocht, S.; Verbiest, T.; Persoons, A.; Kauranen, M.; Phillips, K. E. S.; Katz, T. J. *J. Chem. Phys.* **2000**, *113*, 7578–7581.

JP7114719